

HIGHLY IONIZED CALCIUM AND ARGON X-RAY SPECTRA FROM A LARGE SOLAR FLARE

K. J. H. Phillips¹, J. Sylwester², B. Sylwester², M. Kowaliński², M. Siarkowski²,
W. Trzebiński², S. Płoceniak², Z. Kordylewski²

¹ Earth Sciences Department, Natural History Museum, London SW7 5BD, UK

kennethjhphillips@yahoo.com

² Space Research Centre, Polish Academy of Sciences, Kopernika 11, 51-622 Wrocław, and
Bartycka 18A, 00-716 Warszawa, Poland

bs@cbk.pan.wroc.pl, js@cbk.pan.wroc.pl

Received _____; accepted _____

Submitted to Astrophysical Journal.

ABSTRACT

X-ray lines of helium-like calcium (Ca XIX) between 3.17 Å and 3.21 Å and associated Ca XVIII dielectronic satellites have previously been observed in solar flare spectra, and their excitation mechanisms are well established. Dielectronic satellites of lower ionization stages (Ca XVII – Ca XV) are not as well characterized. Several spectra during a large solar flare in 2001 by the DIOGENESS X-ray spectrometer on the *CORONAS-F* spacecraft show the Ca XVII and Ca XVI satellites as well as lines of ionized argon (Ar XVII, Ar XVI) including dielectronic satellites. The DIOGENESS spectra are compared with spectra from a synthesis code developed here based on an isothermal assumption with various atomic sources including dielectronic satellite data from the Cowan Hartree–Fock code. Best-fit comparisons are made by varying the temperature as the code’s input (Ar/Ca abundance ratio fixed at 0.33); close agreement is achieved although with adjustments to some ion fractions. The derived temperature is close to that derived from the two *GOES* X-ray channels, T_{GOES} . Some lines are identified for the first time. Similar spectra from the *P78-1* spacecraft and the Alcator C-Mod tokamak have also been analyzed and similar agreement obtained. The importance of blends of calcium and argon lines is emphasized, affecting line ratios used for temperature diagnostics. This analysis will be applied to the *Solar Maximum Mission* Bent Crystal Spectrometer archive and to X-ray spectra expected from the ChemiX instrument on the Sun-orbiting *Interhelioprobe* spacecraft, while the relevance to X-ray spectra from non-solar sources is indicated.

Subject headings: atomic data – Sun: abundances — Sun: corona — Sun: flares — Sun: X-rays, gamma rays

1. INTRODUCTION

Highly ionized calcium X-ray spectra have been observed by several instruments on solar spacecraft, particularly those dedicated to the study of high-temperature flare-produced plasmas. Lines due to helium-like Ca (Ca XIX) in the wavelength range $3.17 - 3.21 \text{ \AA}$ occur in flares with *GOES* classifications C1 and higher, and with temperatures of up to $\sim 20 \text{ MK}$. Ca XIX spectra were recorded by SOLFLEX (*Solar Flare X-rays*) on *P78-1* (operating 1979 – 1981), the Bent Crystal Spectrometer on *Solar Maximum Mission* (1980 and 1984 – 1989), and the Bragg Crystal Spectrometer on *Yohkoh* (1991 – 2001), time periods coinciding with the high-activity maxima of Solar Cycles 21 and 22, when unlike much of the most recent cycle (24) *GOES* class M and X flares were commonplace. The Ca XIX lines include the resonance line (line *w*, 3.17735 \AA : notation of Gabriel (1972)), intercombination lines (*x*, 3.18941 \AA ; *y*, 3.19291 \AA), and forbidden line (*z*, 3.21095 \AA) (quoted wavelengths are from SOLFLEX measurements: Seely & Doschek (1989)). Prominent dielectronic satellites emitted by Li-like Ca (Ca XVIII) occur near the Ca XIX lines, with wavelengths mostly between lines *w* and *z*. Other dielectronic satellites, emitted by Li-like Ca (Ca XVII), have been observed in solar flare spectra by SOLFLEX as well as from high-temperature plasmas in the Alcator C-Mod tokamak device (Rice et al. 2014, 2015, 2017).

Here we discuss a very large (*GOES* class X5.3) flare on 2001 August 25 observed by the DIOGENESS scanning crystal spectrometer on the *CORONAS-F* spacecraft. Scans were made over the complete duration of the flare with two of the four channels covering the wavelength region of the Ca XIX lines and Ca XVIII satellites. The spectra were averaged over five time periods each with similar temperature, defined by T_{GOES} derived from the emission ratio of the two channels of *GOES*; details are described in Section 2. During the flare decay stage, when the temperature was lower, lines of lower ionization stages are also evident as are lines of H-like and He-like argon (Ar XVIII, Ar XVII) and associated

dielectronic satellites. We compare the observed spectra with isothermal synthetic spectra over the 3.05 – 3.35 Å range generated by a purpose-written code, developed for this work and described in Section 3, based on various published sources and new calculations of calcium and argon satellite lines made with the Cowan Hartree–Fock atomic code (Cowan 1981). A grid of spectra with a large range of input electron temperatures T_e allowed this comparison to be made. The averaged DIOGENESS spectra over the five temperature intervals were compared with the synthetic spectra calculated for temperature equal to T_{GOES} (Section 4). Most of the spectral features are reproduced with high accuracy although the lower-temperature Ca XVII lines were found to be more intense than calculated. This is attributed to uncertainties in the very small Ca^{+16} ion fractions at these temperatures; increasing these then gives much improved agreement. Justification for this adjustment is provided by trial calculations in which the effect of 10% uncertainties in the ionization and recombination rates on the ion fractions are examined (paper in preparation).

A number of spectral line features – dielectronic satellites of Ca and Ar ions – not previously noted are observed and identified in the DIOGENESS spectra. The synthetic spectra are also compared with published spectra from SOLFLEX during solar flares and with highly ionized calcium spectra obtained from the Alcator C-Mod tokamak device. The present analysis will be applied to solar flare spectra in the *SMM* data archive and to spectra expected from the crystal spectrometer ChemiX (Siarkowski et al. 2016), which is part of the payload of the Sun-orbiting *Interhelioprobe* spacecraft, to be launched in 2025 or 2026.

2. DIOGENESS SPECTRA

2.1. DIOGENESS Instrument and Calibration

The *CORONAS-F* spacecraft was operational between 2001 and 2006, and had a near-polar orbit with period 94.9 minutes, with up to 35-minute spacecraft night periods and occasional interruptions due to passages through enhanced particle radiation associated with the South Atlantic Anomaly and auroral oval regions near each pole. The bent crystal spectrometer RESIK (REntgenovsky Spektrometr s Izognutyimi Kristalami) built by the Space Research Centre (SRC) group obtained solar flare spectra in the 3.36 – 6.05 Å range which have been extensively used for element abundance determinations and other investigations (see Sylwester et al. (2005, 2012) and references therein). The SRC companion DIOGENESS instrument operated for only a few weeks at the beginning of the spacecraft mission, 2001 August 16 to September 17, but in its short lifetime it observed several large flares (for flare list and instrumental details, see Sylwester et al. (2015b)) including an X5.3 flare on 2001 August 25 (SOL2001-08-25T16:45), one of the largest in Solar Cycle 23. DIOGENESS consisted of four quartz crystals mounted on a single rotatable shaft that were rocked back and forth during the observations. Thus, X-rays from a solar flare were incident at various angles θ , giving diffraction at wavelengths λ according to Bragg’s law $\lambda = 2d \sin \theta$ for first-order diffraction (d is the crystal lattice spacing and is equal to 6.6855 Å for the quartz crystals used). The diffracted radiation was detected by double proportional counters, with calibration sources illuminating the rear section of each detector. This type of double proportional counter arrangement was previously used for X-ray detection in solar instruments aboard the *Prognoz* and *Interball-tail* satellites constructed by the SRC group. Channels 2 and 3 of DIOGENESS covered narrow wavelength bands around the resonance lines of S XV (5.04 Å) and Si XIII (6.65 Å) respectively. The August 25 flare spectra discussed here were obtained by channels 1 and

4, including lines of He-like Ca (Ca XIX) with nearby Ca XVIII dielectronic satellite lines (3.17 – 3.21 Å); the wavelength ranges were 3.12 – 3.32 Å (channel 1) and 3.04 – 3.24 Å (channel 4), so the overlapping region (3.12 – 3.24 Å) included the Ca XIX lines. In some spectra, an Fe XXV emission line in second order diffraction, at 3.1463 Å, is apparent. Channels 1 and 4 were arranged in a “Dopplerometer” mode, i.e., with the two crystals (of quartz 10 $\bar{1}$ 1) facing each other such that spatial displacements of the flare emitting region could be distinguished from spectral shifts due to Doppler motions.

An absolute intensity calibration was first established, with the instrument’s effective area A_{eff} (cm²) given by

$$A_{\text{eff}} = A_{\text{window}} \times \kappa_{\text{window}} \times E_{\text{det}} \times R_{\text{int}}, \quad (1)$$

where A_{window} is the detector window area, κ_{window} and E_{det} are the absorption coefficients of the beryllium window and detector gas respectively, and R_{int} the integrated reflectivity of the crystal. Although no pre-launch measurements were made of the detectors, data are available from measurements made on identical flight spares, giving for the Ca XIX line w wavelength (3.176 Å) $\kappa_{\text{window}} = 0.78$, $A_{\text{window}} = 0.2854 \pm 0.006$ cm², and $E_{\text{det}} = 0.57$. An on-line X-ray optics toolkit (XOP: Sanchez del Rio & Dejus (2004)) was used to evaluate R_{int} , which was found to be 3.4×10^{-5} at 3.17 Å for quartz 10 $\bar{1}$ 1 crystal (a re-measured value of a flight spare crystal gave 4.0×10^{-5}). The resulting value of A_{eff} at 3.17 Å was determined to be 4.31×10^{-6} cm², with an estimated uncertainty of 20%. The rotational scanning speed was 56 arcmin s⁻¹ and data gathering interval 0.40125 s.

2.2. DIOGENESS Spectra

Figure 1 (top panel) shows the time variations in the photon count rate of DIOGENESS channels 1 and channel 4, and the *GOES* 1 – 8 Å irradiance (black curve) during the August 25 flare over the period 16:09 – 17:50 UT. A small precursor apparent in both the DIOGENESS and *GOES* data occurred at 16:17 UT, followed by a sharp rise (16:26 – 16:34 UT) to maximum which occurred at about 16:45 UT. The impulsive stage during this sharp rise is marked by hard X-ray (53 – 93 keV) emission observed by the *Yohkoh* Hard X-ray Telescope. The flare decay, with a short minor burst at 17:35 UT, was observed by DIOGENESS until 17:50 UT. A gap in the DIOGENESS data at 16:42 – 16:48 UT is due to a brief loss of telemetry. The DIOGENESS data points show peaks corresponding to the Ca XIX spectral line group as the spectrometer drive scanned back and forth over its range in a period of ~ 140 s. Some 64 channel 1 and 4 spectra were obtained. The lower panel of this figure shows the temperature T_{GOES} derived from the ratio of emission in the two *GOES* channels averaged over short time intervals (indicated by horizontal error bars) with standard deviations (vertical error bars). *Yohkoh* HXT and Soft X-ray Telescope (SXT) images of the flare, which was located in the south–east part of the solar disk (S17 E34), were shown by Sylwester et al. (2015b). The fast-changing morphology of the sources during the initial phase of this flare is discussed by Siarkowski & Falewicz (2004).

As some of the 64 DIOGENESS spectra have low or medium statistical significance, channel 1 and 4 spectra were combined and averaged over time periods that correspond to five intervals when the derived T_{GOES} (in MK) was in the ranges 12–13, 13–14, 14–16, 16–18, and 18–21, with average values (MK) of 12.8, 13.4, 14.8, 16.8, and 20.7. They are shown as logarithmic plots in Figure 2 in spectral irradiance units ($\text{photon cm}^{-2} \text{s}^{-1} \text{Å}^{-1}$) using the calibration data of Section 2.1 (spectra for $T_{\text{GOES}} \geq 12.8$ MK are increased by 0.5 in the logarithm for clarity); the spectral irradiances were divided by the emission measure

EM_{GOES} derived from T_{GOES} . The five intervals exclude the initial flare rise since the plasma conditions could be non-stationary and non-equilibrium. The background in each of the spectra shown is due to fluorescence and secondary emissions related to magnetospheric high-energy particles; analysis of the spectra included this background to preserve as far as possible the integrity of low-intensity spectral features discussed further in this work. The spectral range of channel 1 includes not only the Ca XIX lines and Ca XVIII satellites but also satellites due to lower ionization stages on the long-wavelength side of Ca XIX line z . The short-wavelength part of the channel 4 range includes Ar XVII ($1s^2 - 1snp$, $n = 5, 6, 7, 8$: called here $w5$, $w6$, $w7$, and $w8$) and Ar XVIII ($\text{Ly}\beta$) lines. Dielectronic satellites associated with these lines are also evident, as we shall discuss later.

3. SYNTHETIC SPECTRA

3.1. Calculation

The CHIANTI (v. 8) atomic database and code (Dere et al. 1997; Landi et al. 2006) allow the calculation of Ca XIX spectra and Ca XVIII dielectronic satellites, although refinements to the Ca XIX line intensities and also satellites from Ca XVII and lower ionization stages are not included. These satellites are important in the August 25 flare spectra, so for the purpose of this study we chose to synthesize spectra using a specially written program in Interactive Data Language (IDL), incorporating atomic data from various sources. The calculated spectra include the principal Ca XIX lines, which dominate the spectrum, and dielectronic satellites of Ca XVIII, Ca XVII, Ca XVI, and Ca XV. These satellites are mostly due to $1s - 2p$ transitions in the presence of spectator (non-participating) electrons. Lines of He-like Ar (Ar XVII) lines ($w4$, $w5$, $w6$, and $w7$) and the Ar XVIII $1s - 3p$ ($\text{Ly}\beta$) line were included, as were associated Ar XVI and Ar XVII dielectronic satellites.

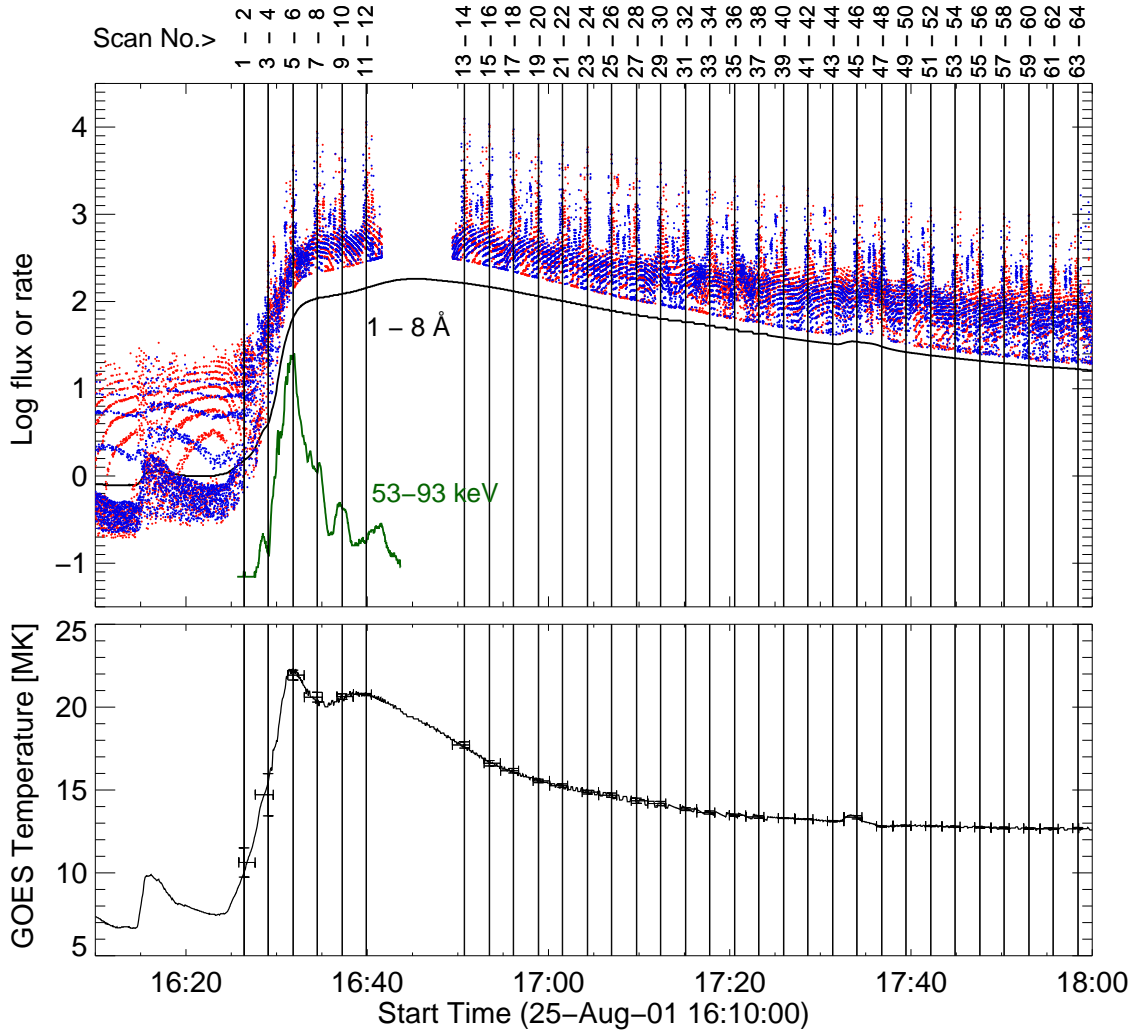


Fig. 1.— Upper panel: Logarithmic plots of *GOES* light curve in the 1–8 Å channel, DIOGENESS channel 1 (red dots) and channel 4 (blue dots), with *Yohkoh* Hard X-ray Telescope (53–93 keV) (green curve) photon count rates during the 2001 August 25 X5 flare are shown. The DIOGENESS points show peaks due to the Ca XIX line group as the crystals repeatedly scanned over their ranges. The data gap between 16:42 UT and 16:49 UT is due to telemetry loss. Lower panel: Temperature derived from the intensity ratio of the two *GOES* channels (horizontal error bars are periods over which averages were obtained, vertical error bars are standard deviations in temperature estimates).

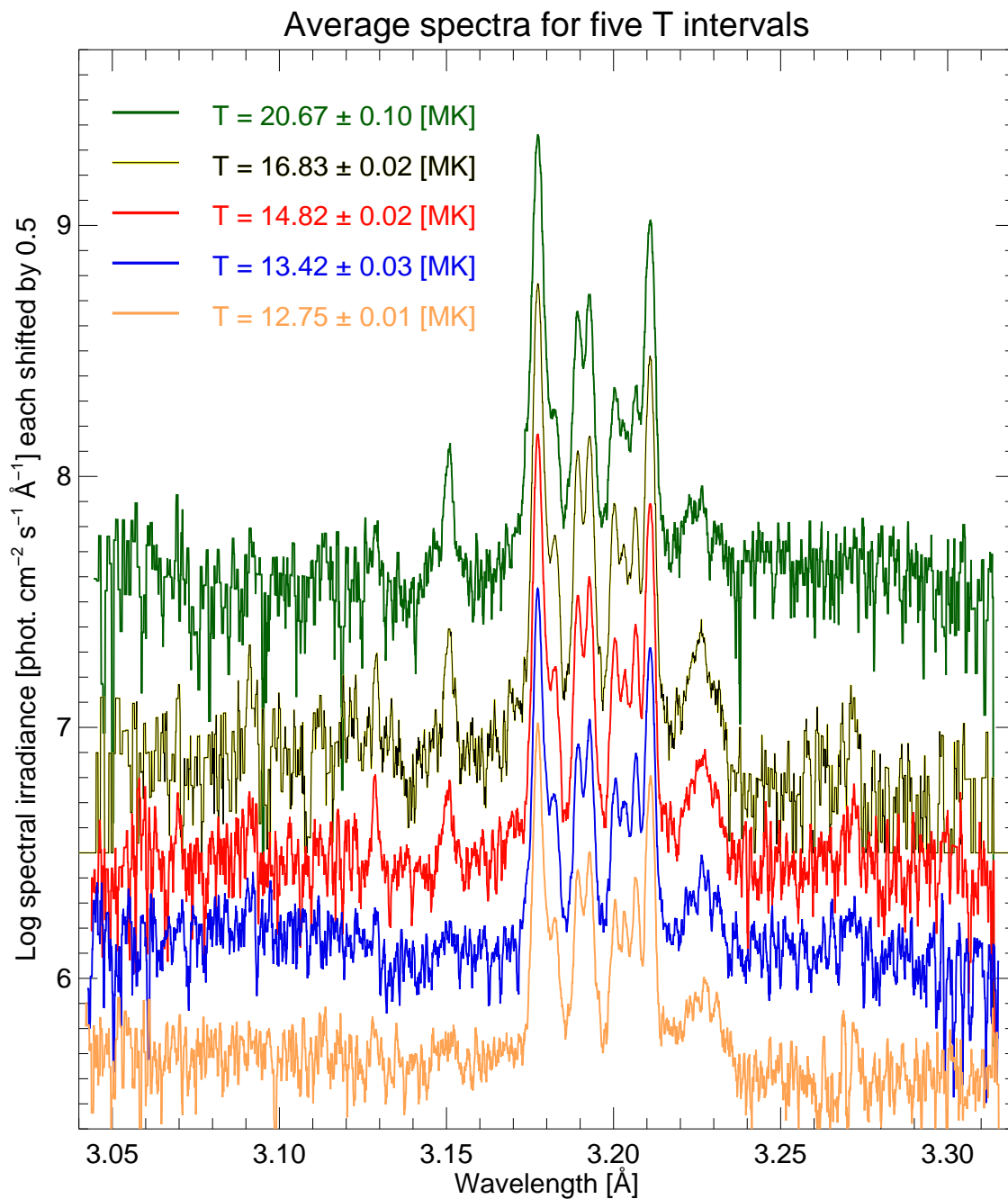


Fig. 2.— DIOGENESS spectra plotted on a logarithmic scale during the 2001 August 25 flare averaged over five time intervals defined by T_{GOES} indicated in the figure legend. The vertical scale units are shown, valid for the $T_{\text{GOES}} = 12.8$ MK spectrum, with successive higher-temperature spectra increased by 0.5 in the logarithm for clarity. See Table 1 for identification of principal spectral features.

A grid of synthetic spectra in the range $3.00 - 3.35 \text{ \AA}$ based on calculated line and continuum intensities was constructed for temperatures $\log T_e = 6.48 - 8.0$ ($T_e = 3 - 100 \text{ MK}$) in 0.02 dex steps and further interpolated in steps of 0.1 MK. Spectra in this grid were compared with observed spectra during the August 25 flare for deducing temperatures on an isothermal assumption. A value of emission measure, $N_e^2 V$ ($N_e =$ electron density, $V =$ emitting volume), was derived from the factor that the synthetic spectrum in spectral irradiance units is multiplied by in order to agree with the observed spectrum. An isothermal assumption is valid for the observed spectra shown in Figure 2, which exclude those in the initial sharp rise in emission. Ionization equilibrium was assumed as is justified for flare plasma densities except when the temperature is rapidly changing. Ion fractions as a function of temperature were taken from CHIANTI v. 8 (Del Zanna et al. 2015) (these are very close to those of Bryans et al. (2009)). From observations with the *SMM* Bent Crystal Spectrometer (Sylwester et al. 1998), the Ca abundance is known to vary from flare to flare; the average value, $A(\text{Ca}) = 6.76$ (log scale with $A(\text{H}) = 12$), was taken for the calculated spectra and for the observed August 25 spectra. For the argon abundance, we took $A(\text{Ar}) = 6.45$ based on an extensive analysis of RESIK flare observations (Sylwester et al. 2010a). Thus the Ar/Ca abundance ratio is 0.33, which is less than the photospheric ratio (0.87: Asplund et al. (2009)), but is accounted for by an expected factor-of-three or more enhancement of elements with low ($\lesssim 10 \text{ eV}$) first ionization potentials (FIPs) including calcium but not argon (see Phillips et al. (2008), chapter 11).

3.2. Ca XIX Lines

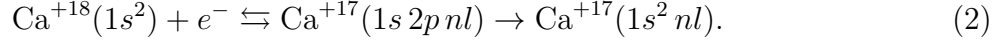
The principal lines of He-like Ca (Ca XIX) are w ($1s^2\ ^1S_0 - 1s2p\ ^1P_1$), x ($1s^2\ ^1S_0 - 1s2p\ ^3P_2$), y ($1s^2\ ^1S_0 - 1s2p\ ^3P_1$), and z ($1s^2\ ^1S_0 - 1s2p\ ^3S_1$). The excitation of these lines is principally by electron collisions; here we used excitation rates from the distorted wave

calculations of Bely-Dubau et al. (1982). These include excitation by recombination from H-like Ca, important at relatively high temperatures (e.g., $\sim 21\%$ contribution to line z at 20 MK), and ionization of Li-like Ca, important at the few per cent level for line z at relatively low ($\lesssim 5$ MK) temperatures. We used the wavelengths of Ca XIX lines from Seely & Doschek (1989), measured from SOLFLEX spectra.

Since the Bely-Dubau et al. (1982) work on Ca XIX collision strength calculations, more detailed close-coupling collision strengths have become available, so comparison with these should be made. The close-coupling calculations of Whiteford et al. (2001) are those used in the CHIANTI software package for the Ca XIX lines, and include radiation damping of the auto-ionizing resonances that are more important for the excitation of Ca XIX lines x , y , and z . The more recent work of Aggarwal & Keenan (2012) shows some differences from Whiteford et al. (2001) although these are only important for ultraviolet transitions. A comparison of the Bely-Dubau et al. (1982) collision strengths for energies between 400 Ry and 800 Ry and those of Aggarwal & Keenan (2012) shows differences that are extremely small, of order 1%, for excitation to the upper level of line w , and only a few percent for other transitions. The largest difference (up to 6%) is for excitation to the upper level of line y . Thus, use of the Bely-Dubau et al. (1982) collision strength data rather than the close-coupling data should result in negligible differences to calculated spectra.

3.3. Ca XVIII – Ca XV Dielectronic Satellites

The theory of the formation of dielectronic satellite lines is given by Gabriel (1972) and applied to Ca XVIII satellites by Bely-Dubau et al. (1982), so we give only brief details here. A Ca XVIII satellite line is formed by the dielectronic capture of a free electron by the He-like ion Ca^{+18} resulting in a doubly excited state of the Li-like ion Ca^{+17} :



The doubly excited state may de-excite either radiatively or by auto-ionization to Ca^{+18} and a free electron (hence the double arrow in Equation 2). If there is radiative de-excitation, satellite lines in the transition array $1s^2\ nl - 1s\ 2p\ nl$ result. The principal $n = 2 - 4$ dielectronic lines cover the wavelength range $3.175 - 3.269\ \text{\AA}$; for increasing n , the satellites converge on the Ca XIX lines.

Following Gabriel (1972), the satellite line irradiance at the distance of the Earth (I_s : photon $\text{cm}^{-2}\ \text{s}^{-1}$) is

$$I_s = \frac{N_e N(\text{Ca}^{+18}) V}{4\pi (\text{AU})^2} \frac{2.06 \times 10^{-16} F_s \exp(-E_s/k_B T_e)}{g_1 T_e^{3/2}} \quad [\text{photons cm}^{-2}\ \text{s}^{-1}], \quad (3)$$

where E_s is the excitation energy of the line's upper state above the ground state of the He-like ion and g_1 the statistical weight of the ground level ($1s^2\ ^1S_0$) of Ca^{+18} (so $g_1 = 1$). k_B is Boltzmann's constant, and $N(\text{Ca}^{+19})$ is the number density of He-like Ca ions. The satellite intensity factor F_s is given by

$$F_s = \frac{g_s A^r A^a}{A^a + \sum A^r}, \quad (4)$$

where A^r and A^a are transition probabilities from the satellite's upper state by radiation and autoionization respectively and g_s the statistical weight of the upper level of the satellite line transition. The summation is of radiative transition probabilities from the upper state to all possible lower states.

Values of F_s and wavelengths for the Ca XVIII satellites are available from Bely-Dubau et al. (1982) and a number of other works (e.g., Vainshtein & Safronova

(1978)). Here, for consistency with calculations of satellites of lower ionization stages, apart from a few exceptions we used the Cowan Hartree–Fock atomic code (Cowan 1981) to calculate the necessary data. This code was run previously in studies we made of X-ray dielectronic satellites of Li-like K and Cl seen with the RESIK instrument (Sylwester et al. 2010b, 2011). The code¹, outlined in Cowan (1981) (Chapters 8 and 16) and described in more detail by Merts et al. (1976), calculates energy levels and radiative and autoionization probabilities using Slater–Condon theory with pseudo-relativistic corrections. It has been adapted for personal computers (A. Kramida, private communication, 2014) which was how the code was run for this work. The code accepts input for a given satellite line array with scale factors for Slater parameters, specified in recent updates to the program; the output includes values for excitation energies, wavelengths, oscillator strengths, transition probabilities, and F_s for optically allowed transitions. This restriction excludes the Ca XVIII satellites o and p (3.2688 Å, 3.2636 Å) for which the transitions are optically forbidden; for these we used the data of Bely-Dubau et al. (1982). The Cowan calculations were carried out for Ca XVIII satellite arrays $1s^2nl - 1s2pnl$ with n up to 6 and all possible l values. The absolute wavelengths are stated by Merts et al. (1976) to be accurate to about 0.2% for transitions considered here, i.e., about 6 mÅ. Our calculations of absolute wavelengths indicate a higher precision is achieved; the Cowan wavelengths are generally less than both those of Seely & Doschek (1989) measured from *P78-1* SOLFLEX spectra and those of Rice et al. (2014) measured from Alcator C-Mod tokamak spectra by an amount $\Delta\lambda$ between 2 mÅ and 4 mÅ, with an average value of $\Delta\lambda = 3.2$ mÅ. This amount was added to the Cowan wavelengths in the synthesis code. It was checked with runs of the Cowan code for satellites with very high n which converge on the Ca XIX

¹The Cowan atomic program package is currently hosted at Trinity College Dublin: <https://www.tcd.ie/Physics/people/Cormac.McGuinness/Cowan/>

lines w , x , and y , giving $\Delta\lambda \approx 3 \text{ m}\text{\AA}$. An exception is the medium-importance satellite m for which the Cowan wavelength (3.1926 \AA) is more than the calculated wavelengths of Bely-Dubau et al. (1982) (3.1880 \AA) and Vainshtein & Safronova (1978) (3.1890 \AA) by about 4 $\text{m}\text{\AA}$. Laser plasma X-ray wavelength measurements by Feldman et al. (1974) for various He-like ion spectra show that the wavelength is near that of Bely-Dubau et al. (1982), and accordingly this wavelength was adopted here. Note that in all solar and Alcator spectra, the highest-intensity satellite j is indistinguishable from Ca XIX line z .

Satellites of Ca XVII, Ca XVI, and Ca XV were similarly calculated with the Cowan code. These satellites occur to the long-wavelength side of Ca XIX line z ($\gtrsim 3.21 \text{ \AA}$). Their intensities are given by Equations (3) and (4) with $g_1 = 2$ for Ca XVII satellites (excitation from the ground level $1s^2 2s^2 S_{1/2}$ of Ca^{+17} with statistical weight 2), 1 for Ca XVI (excitation from $1s^2 2s^2 {}^1S_0$ of Ca^{+16}), and 2 for Ca XV (excitation from $1s^2 2s^2 2p^2 P_{1/2}$ of Ca^{+15}). Several Ca XVII satellites are particularly prominent in the DIOGENESS solar spectra as well as in the flare spectra of Seely & Doschek (1989) and the Alcator spectra of Rice et al. (2014); we took the measured wavelengths of these from Seely & Doschek (1989). (Lines with identical transitions are also seen in solar flare Fe XXIII spectra: Lemen et al. (1984).) The Cowan wavelengths for the same lines are smaller by $\sim 3 \text{ m}\text{\AA}$, i.e., a similar amount to that of the Ca XVIII satellites, so for the remaining satellites, 3.2 $\text{m}\text{\AA}$ was added to the Cowan wavelengths.

Table 1 gives data for important lines of calcium ions included in the spectral synthesis program, including line notation and transitions, wavelengths adopted and measured (Seely & Doschek (1989); Rice et al. (2014)). The line notation is from Gabriel (1972) for the Ca XIX and Ca XVIII lines, and from Seely & Doschek (1989) for the Ca XVII satellite features seen in SOLFLEX spectra. Table 1 also gives, for the dielectronic satellites, values of F_s from the Cowan program and for comparison values from either Vainshtein & Safronova

(1978) or Safronova & Lisina (1979). Approximately 2000 other weaker satellites of calcium ions are included in the program. There is $\sim 10\%$ agreement between the Cowan F_s values and those of Vainshtein & Safronova (1978) or Safronova & Lisina (1979) for the more intense satellites ($F_s \gtrsim 10^{14} \text{ s}^{-1}$); for weaker satellites, a factor-of-two agreement is more typical. Such errors should not affect the general appearance of the spectrum. Note that neither this table, nor our calculations, includes the Fe XXV line (transition $1s^2 1S_0 - 1s3p^1P_1$) with wavelength 1.5731 \AA (observed in second diffraction order at 3.1463 \AA) which is apparent in high-temperature DIOGENESS spectra.

Inner-shell excitation is significant for several Ca XVIII satellites, notably $o - v$. For these satellites, we used the collisional excitation rates calculated by Bely-Dubau et al. (1982). The excitation of the Ca XVII β line (transition $1s^2 2s^2 1S_0 - 1s 2s^2 2p^1P_1$) is also significant, but no published data for the collision excitation rates currently exist. However, temperature-averaged collision strengths for this and the $1s^2 2s^2 1S_0 - 1s 2s^2 2p^3P_1$ transition have been calculated by Mann (1983) for Fe XXIII, the equivalent Fe ion. Z -scaling laws ($Z =$ atomic number) given by Burgess & Tully (1992) were used to calculate temperature-averaged collision strengths for Ca XVII line β , from which excitation rates were derived. For a broad temperature range, the dielectronic and inner-shell contributions to this line are comparable. Although the F_s value used here differs from that of Safronova & Lisina (1979) (Table 1), there is little effect on the total intensity of this line. Inner-shell contributions to some other Ca XVI and Ca XV lines are possible but are much smaller and have been neglected.

The convergence of the high- n satellites calculated here is illustrated by Figure 3, showing the summed contribution of satellites with $n = 3, 4, 5,$ and 6 near Ca XIX line w calculated for $T = 13.8 \text{ MK}$. For this temperature, we estimate that the total emission within 1.15 m\AA of the central wavelength of Ca XIX line w , 8.6% is due to unresolved

$n = 3$ satellites, 1.4% to $n = 4$ satellites, 2.3% to $n = 5$ satellites, and 2.1% to $n = 6$ satellites. Using the data of Bely-Dubau et al. (1982), the contribution of $n > 7$ satellites is approximately 1.6%.

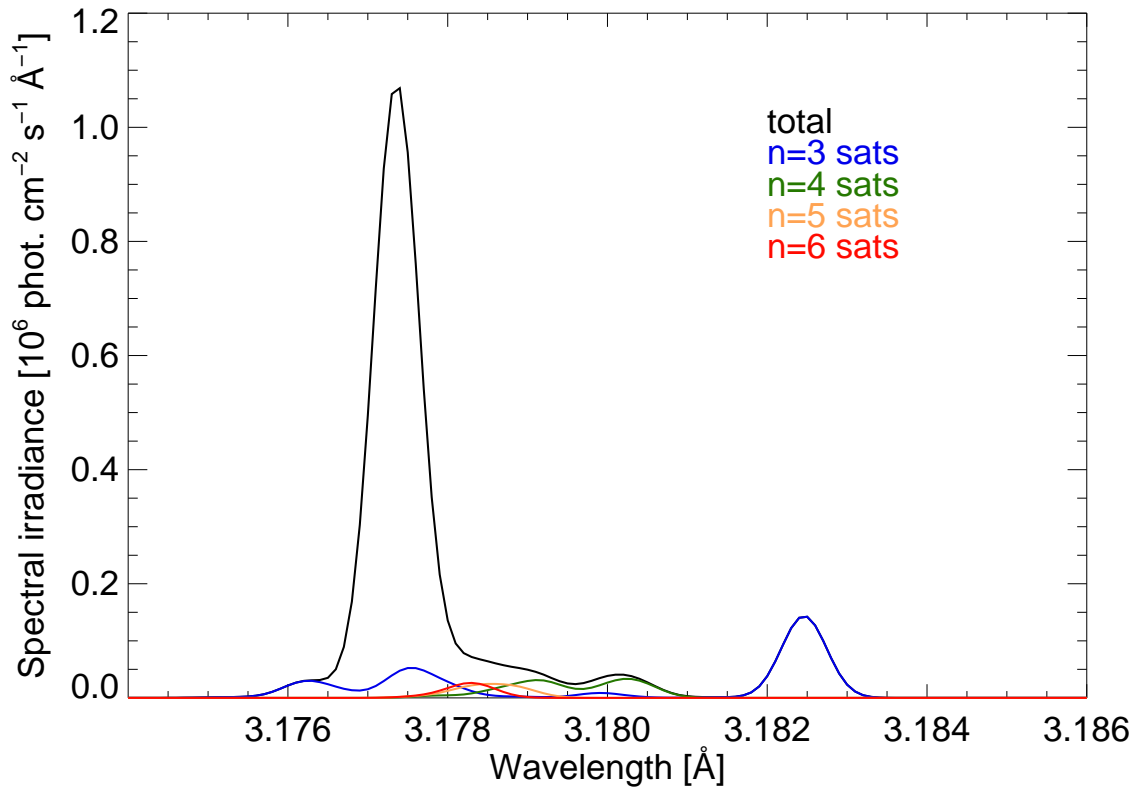


Fig. 3.— Convergence of high- n dielectronic satellites on to the Ca XIX w line: theoretical spectrum for $T = 13.8$ MK. Each satellite group is color-coded, and the key indicated in the legend.

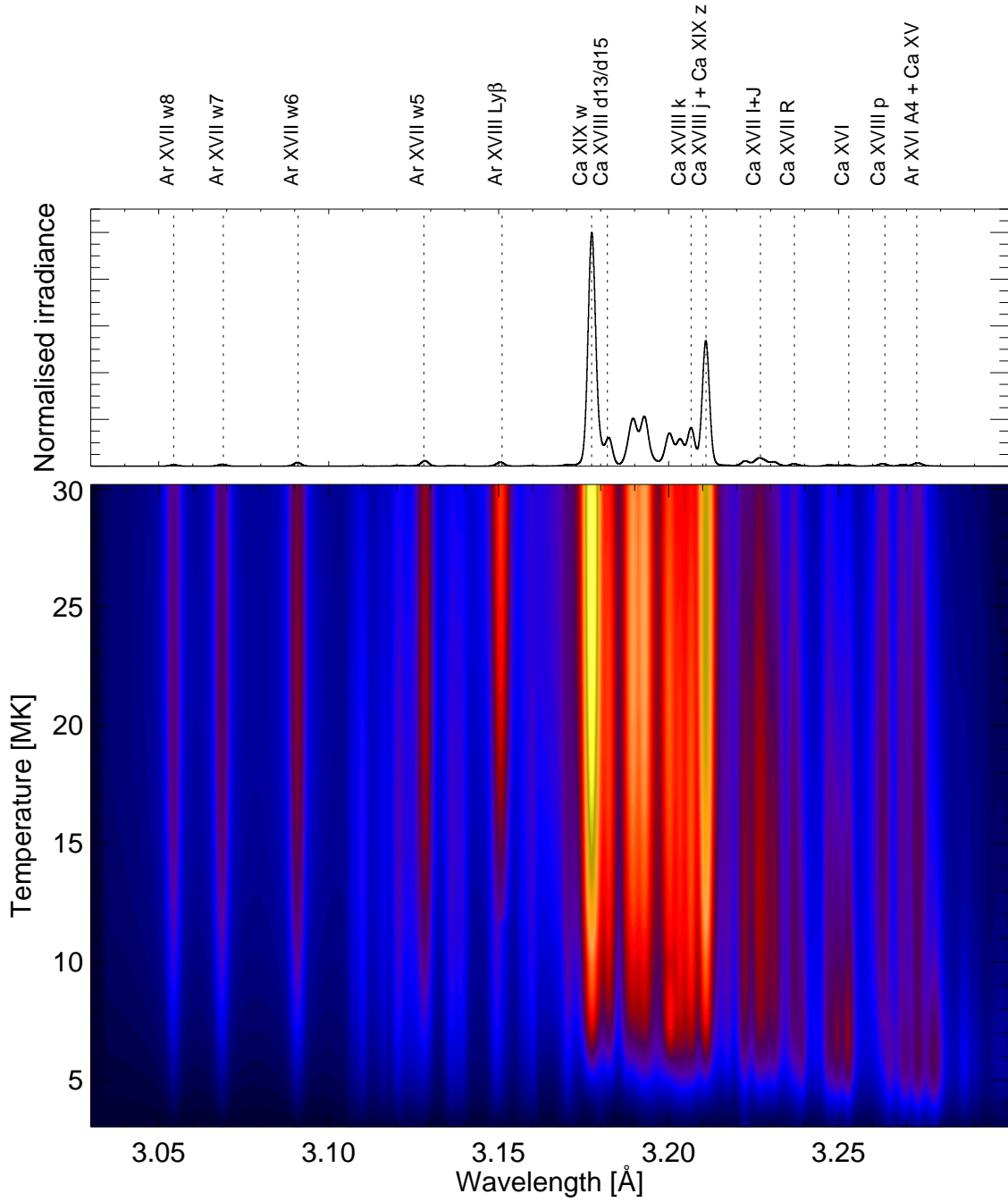


Fig. 4.— Synthetic spectra in the range 3.00 – 3.30 Å for temperatures in the range 4 MK (bottom) to 30 MK (top), color-coded with blue, orange, red, yellow indicating increasing intensities. The chief lines are identified at the top of the figure with a theoretical spectrum with temperature equal to 13.8 MK. (For line widths, see text.)

Table 1. Principal Lines in the range 3.00–3.30 Å.

Ion	Transition	Key ^a	Wavel. (Adopted) ^b	Wavel. (Measured) ^c	$F(s)^d$ (s ⁻¹)	$F(s)^e$ (s ⁻¹)	$F(s)^f$ (s ⁻¹)
Ar XVII	$1s^2 1S_0 - 1s 8p^1 P_1$	<i>w</i> 8	3.0544	3.0544			
Ar XVII	$1s^2 1S_0 - 1s 7p^1 P_1$	<i>w</i> 7	3.0686	3.0686			
Ar XVII	$1s^2 1S_0 - 1s 6p^1 P_1$	<i>w</i> 6	3.0908	3.0908			
Ar XVII	$1s^2 1S_0 - 1s 5p^1 P_1$	<i>w</i> 5	3.12834	3.12834			
Ar XVI	$1s^2 2p^2 P - 1s 2p 8p (^3 P)^2 D$	A8	3.1361	3.135	5.12(12)	4.18(12)	
Ar XVI	$1s^2 2p^2 P - 1s 2p 7p (^3 P)^2 D$	A7	3.1495	3.146	7.89(12)	6.13(12)	
Ar XVIII	$1s^2 S_{1/2} - 2p^2 P_{1/2,3/2}$	Lyβ	3.15062	3.15062			
Ar XVI	$1s^2 2p^2 P - 1s 2p 6p (^3 P)^2 D$	A6	3.1704	3.169	1.31(13)	1.08(13)	
Ca XIX	$1s^2 1S_0 - 1s 2p^1 P_1$	<i>w</i>	3.17735	3.17735	3.1773		
Ca XVIII	$1s^2 4p^2 P - 1s 2p 4p^2 D$	<i>n</i> = 4	3.1802	3.17926	9.89(13)		
Ca XVIII	$1s^2 3p^2 P - 1s 2p 3p (^1 P)^2 D$	<i>d</i> 15, <i>d</i> 13	3.1818	3.1824	3.14(14)		5.55(14)
Ca XVIII	$1s^2 2p^2 P_{3/2} - 1s 2p^2 2S_{1/2}$	<i>m</i>	3.1880		7.03(13)	4.10(13)	2.99(13)
Ca XIX	$1s^2 1S_0 - 1s 2p^3 P_2$	<i>x</i>	3.18941	3.18941			
Ca XVIII	$1s^2 2s^2 S_{1/2} - 1s 2s 2p (^3 P)^2 P_{3/2}$	<i>s</i>	3.1902	3.1869	3.00(13)	1.74(13)	2.61(13)
Ca XVIII	$1s^2 2s^2 S_{1/2} - 1s 2s 2p (^3 P)^2 P_{1/2}$	<i>t</i>	3.1912	3.19113	5.34(13)	5.26(13)	5.31(13)
Ca XIX	$1s^2 1S_0 - 1s 2p^3 P_1$	<i>y</i>	3.19291	3.19291			
Ar XVII	$1s^2 1S_0 - 1s 4p^1 P_1$	<i>w</i> 4	3.1997	3.1997			
Ca XVIII	$1s^2 2s^2 S_{1/2} - 1s 2s 2p (^2 P)^2 P_{3/2}$	<i>q</i>	3.20048	3.20048	1.06(13)	2.68(12)	8.51(11)
Ca XVIII	$1s^2 2s^2 S_{1/2} - 1s 2s 2p (^2 P)^2 P_{1/2}$	<i>r</i>	3.20332	3.20332	3.27(13)	2.88(13)	3.18(13)
Ca XVIII	$1s^2 2p^2 P_{3/2} - 1s 2p^2 2P_{3/2}$	<i>a</i>	3.20332	3.20332	5.93(13)	7.48(13)	5.33(13)
Ar XVI	$1s^2 2p^2 P - 1s 2p 5p (^3 P)^2 D$	A5	3.2058	3.202	2.37(13)	1.93(13)	
Ca XVIII	$1s^2 2p^2 P_{1/2} - 1s 2p^2 2D_{3/2}$	<i>k</i>	3.20663	3.20663	2.34(14)	2.48(14)	2.27(14)
Ca XVIII	$1s^2 2p^2 P_{3/2} - 1s 2p^2 2D_{5/2}$	<i>j</i>	3.21095	3.21095	3.21(14)	3.33(14)	3.10(14)
Ca XIX	$1s^2 1S_0 - 1s 2s^3 S_1$	<i>z</i>	3.21095	3.21095			
Ca XVII	$1s^2 2s 2p^3 P_2 - 1s 2s 2p^2 (^1 S)^3 S_1$	G	3.2171	3.21724	5.59(13)	4.43(13)	
Ca XVII	$1s^2 2s^2 1S_0 - 1s 2s^2 2p (^2 S)^1 P_1$	β	3.221	3.2217	6.14(12)	1.32(14)	
Ca XVIII	$1s^2 2s^2 S_{1/2} - 1s 2s 2p^4 P_{3/2}$	<i>u</i>	3.2264	3.2266	4.29(11)	5.68(11)	4.37(11)
Ca XVII	$1s^2 2s 2p^3 P_0 - 1s 2s 2p^2 (^1 D)^3 D_1$	J	3.22645	3.22645	9.53(13)	1.76(14)	
Ca XVII	$1s^2 2s 2p^3 P_1 - 1s 2s 2p^2 (^1 D)^3 D_1$	I?	3.2265		1.13(14)	1.18(14)	
Ca XVII	$1s^2 2s 2p^3 P_2 - 1s 2s 2p^2 (^3 P)^3 P_2$	L	3.22645?	3.22645	1.30(14)	2.35(14)	
Ca XVIII	$1s^2 2s^2 S_{1/2} - 1s 2s 2p^4 P_{1/2}$	<i>v</i>	3.2279	3.2277	6.56(10)	1.19(12)	3.3(10)
Ca XVII	$1s^2 2s 2p^3 P_1 - 1s 2s 2p^2 (^1 D)^3 D_2$	K	3.22827?	3.22827	2.80(14)	3.14(14)	
Ca XVII	$1s^2 2s 2p^3 P_2 - 1s 2s 2p^2 (^1 D)^3 D_1$		3.2293		5.26(13)		
Ca XVII	$1s^2 2s 2p^3 P_2 - 1s 2s 2p^2 (^1 D)^3 D_3$	N	3.23100?	3.23100	3.65(14)	3.99(14)	
Ca XVII	$1s^2 2s 2p^1 P_1 - 1s 2s 2p^2 (^3 P)^3 P_2$		3.2331		5.28(13)		
Ca XVII	$1s^2 2s 2p^1 P_1 - 1s 2s 2p^2 (^1 D)^1 D_2$	R	3.23677	3.23677	1.95(14)	2.14(14)	
Ca XVI	$1s^2 2s^2 2p^2 P_{1/2} - 1s 2s^2 2p^2 (^1 D)^2 D_{3/2}$		3.2497		2.94(14)		
Ca XVI	$1s^2 2s^2 2p^2 P_{3/2} - 1s 2s^2 2p^2 (^1 D)^2 D_{5/2}$		3.2527		3.78(14)		
Ca XVIII	$1s^2 2p^2 P_{1/2} - 1s 2s^2 2S_{1/2}$	<i>p</i>	3.2636		5.79(12) ^b	5.38(12)	5.79(12)
Ca XVIII	$1s^2 2p^2 P_{3/2} - 1s 2s^2 2S_{1/2}$	<i>o</i>	3.2688		8.27(12) ^b	7.62(12)	8.27(12)
Ar XVI	$1s^2 2p^2 P - 1s 2p 4p (^3 P)^2 D$	A4	3.2731	3.270	4.47(13)	3.12(13)	
Ca XV	$1s^2 2s^2 2p^2 1D_2 - 1s 2s^2 2p^3 (^2 D)^1 D_2$		3.2734		6.95(14)		

^aNotation as follows: Ca XIX, Ca XVIII lines, Gabriel (1972); Ca XVII lines, Seely & Doschek (1989); Ar XVII lines, see text; Ar XVI lines, Rice et al. (2017).

^bAdopted wavelengths: measured (col. 5) or Cowan $\lambda + 0.0032 \text{ \AA}$. For Ca XVIII sats. m, p, o : Bely-Dubau et al. (1982). For Ar XVIII Ly β λ : Erickson (1977). Intensity factor (F_s , Eq. 4) for p, o : Bely-Dubau et al. (1982).

^cMeasured wavelengths: SOLFLEX (Seely & Doschek 1989) or Alcator C-Mod tokamak (Rice et al. 2017).

^dIntensity factor: Calculated here with Cowan code.

^eIntensity factor: Vainshtein & Safronova (1978) or Safronova & Lisina (1979). Ar XVI lines: Rice et al. (2017).

^fIntensity factor: Bely-Dubau et al. (1982).

3.4. Ar XVII and Ar XVIII lines and satellites

The Ar XVIII $\text{Ly}\beta$ and the Ar XVII $w4$, $w5$, $w6$, $w7$, and (very weakly) $w8$ lines are evident in the higher-temperature DIOGENESS spectra and are included in Table 1. We used CHIANTI v. 8 for the intensities of the $w4$ and $w5$ lines and Rice et al. (2017) from Alcator C-Mod tokamak spectra measurements and theory for the line wavelengths. Ar XVI dielectronic satellites associated with the Ar XVII $w4 - w8$ lines, although relatively weak, are relevant for analysis of DIOGENESS spectra as some blend with the Ca XIX line group. The Ar XVI satellites have transitions $1s^2nl - 1snln'l'$ where nl are quantum numbers for the spectator electron and with n' (the principal quantum number of the jumping electron) equal to 4 to 8. They have been observed and analyzed in Alcator C-Mod tokamak plasma spectra (Rice et al. 2014, 2015), with calculations of wavelengths and intensity factors F_s given by Rice et al. (2017). Generally, two of the most intense Ar XVI satellite transitions, with transitions $1s^2 2p^2 P_{1/2} - 1s 2p n' p^2 D_{3/2}$ and $1s^2 2p^2 P_{3/2} - 1s 2p n' p^2 D_{5/2}$, dominate, making up what is essentially a single line feature (called by Rice et al. (2017) A4, A5, A6, A7, A8 for $n' = 4, 5, 6, 7, 8$: this notation is used in Table 1). Here, wavelengths and F_s values were calculated for these and other satellites with n' up to 12 using the Cowan code, with 3.2 mÅ added to the Cowan wavelengths as with the calcium satellites. As can be seen from Table 1, there is good agreement for both the wavelengths and F_s factors between the Cowan values and those of Rice et al. (2017) for the A4 to A8 satellites. Additional Ar XVI satellite data were calculated with the Cowan code for satellites having transitions $1s^2 2l - 1s 2l nl$ with nl up to $12p$. Wavelengths and F_s values of the Ar XVII dielectronic satellites (transitions $1s2s - 2s3p$, $1s2p - 2p3p$) associated with the Ar XVIII $\text{Ly}\beta$ were similarly calculated with the Cowan code and included in the synthetic spectra. Even the most intense of these satellites were found to make a very small contribution to the total spectrum.

Among the blends of argon lines or dielectronic satellites with the calcium lines, the most significant is that of the Ar XVII $w4$ line (3.200 Å) which is blended with Ca XVIII satellite q (as was noted in *P78-1* spectra: Doschek & Feldman (1981)); for the assumed Ar/Ca abundance ratio of 0.33, the lines are comparable in intensity over a wide temperature range. The Ar XVI A5 satellite line feature is blended with Ca XVIII satellite k , although it makes a less than $\sim 2\%$ contribution to line k . Both Ca XVIII satellites q and k have been extensively used as diagnostics of electron and ion temperature in *SMM* BCS spectral analyses, so the blend of Ca XVIII satellite q and the Ar XVII $w4$ line should be taken into account. The Ar XVI A6 feature is on the short-wavelength wing of the Ca XIX w line; the presence of a line at this wavelength was noticed in some *SMM* BCS spectra but was not then previously identified.

3.5. Continuum

The continuum, made up of free–free, free–bound, and two-photon radiation, was calculated from CHIANTI routines and added to the line spectra, although in the analysis of the DIOGENESS spectra we compared only the line spectra as the DIOGENESS spectra have a continuous background which is mostly instrumental in origin. The continuum calculation used element abundances of Feldman (1992) and ion fractions from the CHIANTI ionization equilibrium. Typically, free-bound emission is comparable to free–free emission over the 3.00 – 3.35 Å range, but two-photon emission is over two orders of magnitude lower.

3.6. Synthetic Spectra Displayed

Figure 4 shows a color-coded representation of synthetic 3.00–3.30 Å spectra for temperatures in the range 4 – 30 MK, with chief lines identified in the spectrum at the top, calculated for 13.8 MK. In these spectra, the line profile was taken to be Gaussian with width equal to the thermal Doppler broadening ($\text{FWHM} = 2.15 \times 10^{-7} T_e^{1/2}$ Å for calcium spectra in this wavelength range) convolved with the DIOGENESS rocking curve and a turbulent velocity of 100 km s⁻¹ to take account of non-thermal broadening. For the lower temperatures (nearest the bottom of the figure), the Ca XVI and Ca XV satellites at longer wavelengths predominate, but rapidly fade with increasing temperature. Correspondingly, the Ca XIX line intensities increase with temperature until ~ 16 MK when the ion fraction of He-like Ca maximizes. The principal Ca XVIII satellites q , $r + a$, k and $d13 + d15$ are also prominent at lower temperatures; for the dielectronically formed lines, their intensities decrease with an approximately T_e^{-1} dependence relative to Ca XIX line w . There is a similar decrease in the intensities of the Ca XVII satellites on the long-wavelength side of Ca XIX line z , reflecting the decreasing proportion of the associated ion fractions with temperature.

4. DIOGENESS AND THEORETICAL SPECTRA COMPARED

4.1. DIOGENESS Solar Flare Spectra

We compared the DIOGENESS spectra in Figure 2 with synthetic spectra calculated for temperatures equal to the appropriate value of T_{GOES} . In the spectrum with the lowest temperature ($T_{\text{GOES}} = 12.8$ MK), the low-temperature Ca XVII satellite lines are most evident while the higher-temperature Ar XVII and Ar XVIII are weak or non-existent. Fitting with theoretical spectra for this temperature should therefore best illustrate the

reliability of the Cowan calculations of the calcium satellites. Figure 5 (left panel) shows the DIOGENESS spectrum with the best-fit theoretical spectrum; the background “pedestal” in the observed spectrum is fitted with an arbitrary background in the theoretical spectrum, and only the theoretical line spectrum without the continuum has been fitted to those in the observed spectrum. It is clear that the Ca XVII lines in the 3.21 – 3.24 Å, particularly Ca XVII line β (3.2217Å), have intensities that are underestimated in the theoretical spectrum, and the weak emission in the 3.24 – 3.25Å in the observed spectrum is not matched by the Ca XVI line emission in the theoretical spectrum. The reduced χ^2 for this fit is 0.79, and the residuals in the form $\log(O/C)$ (O = observed, C = calculated), which are plotted beneath the spectrum, are larger for the wavelength range of the Ca XVII lines.

The Ca XVII line β is partly formed by inner-shell excitation from the Ca^{+16} ion, the remaining Ca XVII line emission by dielectronic recombination of Ca^{+17} ions. Similarly, the weak Ca XVI line emission is formed by dielectronic recombination of Ca^{+16} ions. At a temperature of 12.8 MK, according to the CHIANTI ionization equilibrium calculations used here, the ion fractions of Ca^{+17} and Ca^{+16} are 0.13 and 0.02 respectively, decreasing sharply with temperature. In a separate work in preparation, we examine the likelihood of considerable errors in the ion fractions when small as a result of uncertainties in the ionization and recombination rates. These are generally based on theory with very few benchmark laboratory measurements. Bryans et al. (2006) in an extensive discussion of ionization equilibria finds that the agreement of calculated and measured dielectronic recombination rates is 35% or better, which is probably the typical agreement for other ionization or recombination rates. Our work indicates that an uncertainty of as small as 10% in these rates leads to uncertainties in some ion fractions that are considerable, especially (as in the case of Ca^{+17} and Ca^{+16} at $T_e \gtrsim 12.8$ MK when the ion fractions are very small. In view of this, it seemed to us quite possible that the Ca^{+16} and Ca^{+17} ion fractions should be increased. The factors we used, equal to 1.3 and 2.0 respectively, were

assumed to apply for the whole temperature range of the DIOGENESS spectra considered here (12.8 – 20.7 MK). This arbitrary assumption is not exact since it ignores the fact that the Ca^{+18} ion fractions should be correspondingly adjusted, although since these fractions are nearly unity (between 0.82 and 0.72), the amount is slight. It is found that, with these adjusted ion fractions, the agreement between the DIOGENESS and theoretical spectra is much improved, as is shown by the fits to the Ca XVII lines in Figure 5 (right panel). In addition, the weak emission at 3.24 – 3.25 Å in the observed spectrum can now be identified with the Ca XVI dielectronic lines. (Table 1 gives the two most intense lines.) We found, however, that the reduced χ^2 in this fit (0.79) is almost identical to the fit in Figure 5 (left panel).

It is clear from Figure 5 that the Ar XVII lines make a substantial contribution (blue line in figure). At 12.8 MK, only the Ar XVII $w5$ is prominent on the short-wavelength side of the Ca XIX line w , where there is agreement of the theoretical spectrum with the observed. The $w4$ line is not evident because of the blend with the Ca XVIII satellite q (3.2005 Å), but its intensity calculated on the assumption of an Ar/Ca abundance of 0.33 is 25% of the total intensity of this blended feature. At wavelengths longer than Ca XIX line z (3.211 Å), the Ar XVI satellites seen in Alcator C-Mod tokamak spectra, including the A4 line feature, are visible, as are the Ca XVIII o and p satellites. This is the first time these lines as well as the Ca XVI satellites have been noted in astrophysical spectra.

With the adjustments in Ca XVII and Ca XVI ion fractions from the fits at a temperature of 12.8 MK, we fitted the spectra for the remaining temperatures (13.4 MK, 14.8 MK, 16.8 MK, 20.7 MK), obtaining satisfactory fits for the first two with values of reduced χ^2 of 1.06 and 1.13. Figure 6 shows these four spectra, which have the same color code as Figure 5. For the two higher temperatures, reduced χ^2 was 1.97 and 3.33, the slightly worse fit apparently arising from the noisier background which may be due to

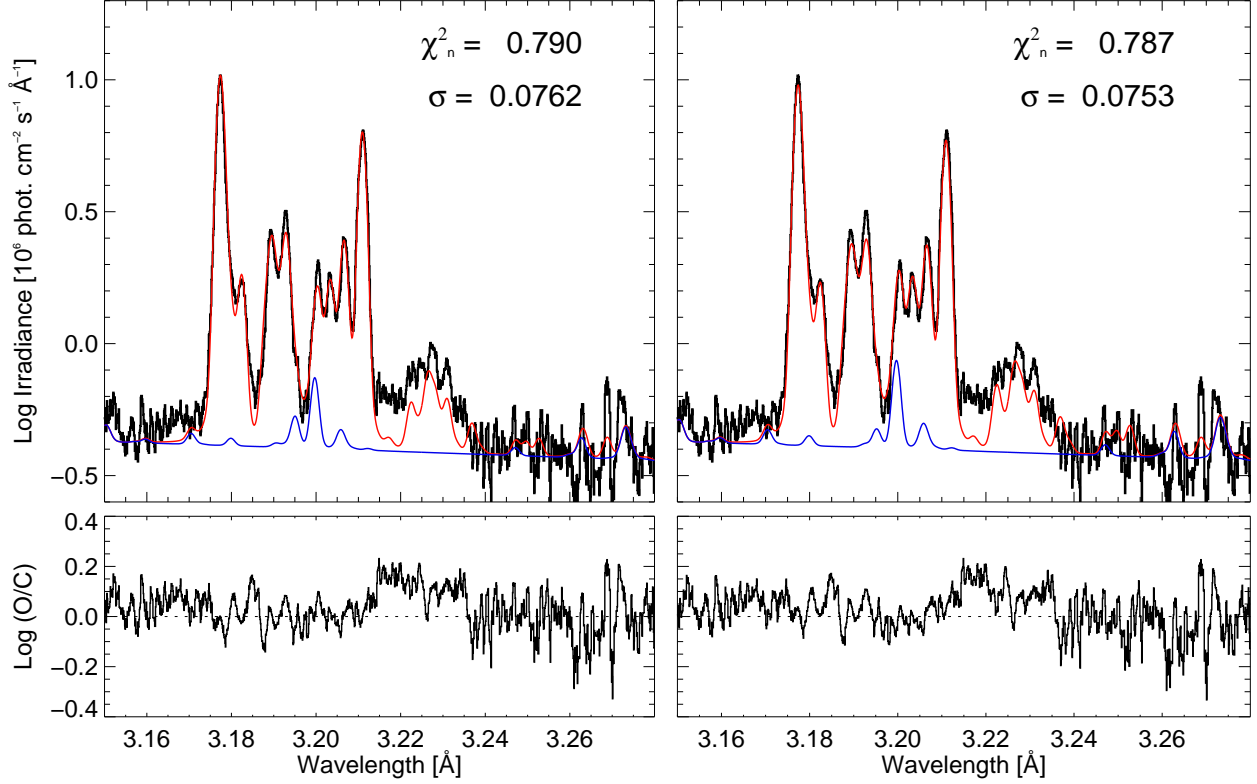


Fig. 5.— (Left) DIOGENESS spectrum for $T_{\text{GOES}} = 12.8$ MK with best-fit theoretical spectrum (red continuous line) on a logarithmic scale, with contribution made by the argon spectrum alone (blue line); fit residuals are shown in the panel beneath. Line identifications may be found in Table 1. The ion fractions given in CHIANTI were used for the theoretical spectrum, and an Ar/Ca abundance ratio equal to 0.33 (Section 3.1). For this fit the reduced $\chi^2 = 0.79$; the largest residuals occur in the region of the Ca XVII lines (3.21 – 3.23 Å). (Right) As for the left panel but with the Ca^{+16} and Ca^{+17} ion fractions multiplied by 1.3 and 2.0 respectively. The Ca XVII lines in the theoretical spectrum agree better, including line β (3.2217Å), as does the weak Ca XVI line emission (3.24 – 3.25Å), although χ^2 is nearly identical.

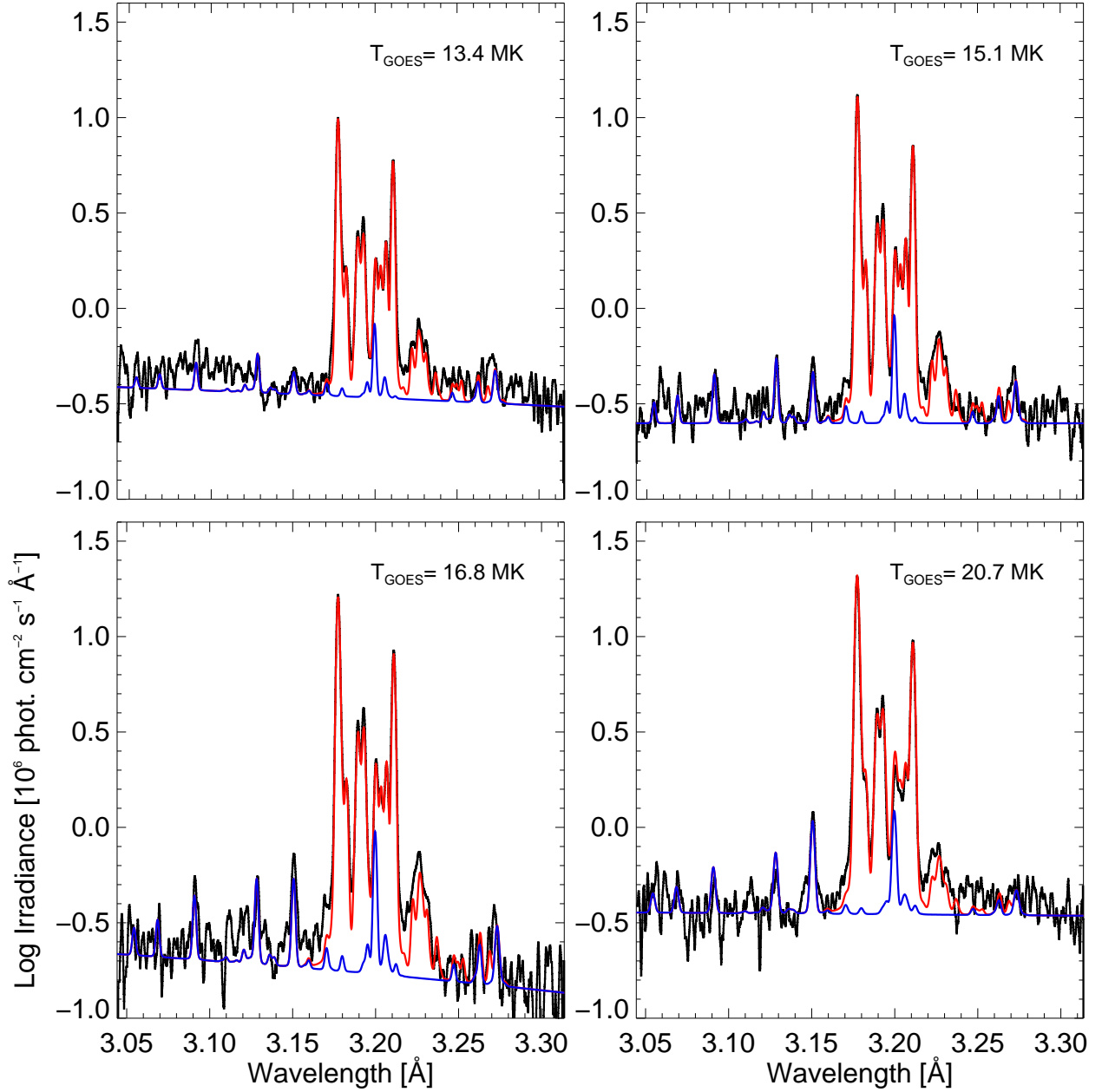


Fig. 6.— DIOGENESS spectra in the range 3.05 – 3.30 Å for $T_{\text{GOES}} = 13.4$ MK, 14.8 MK, 16.8 MK, and 20.7 MK with best-fit theoretical spectra (red continuous line) with argon spectrum (blue line). The Ca^{+16} and Ca^{+17} ion fractions were multiplied by 1.3 and 2.0 respectively as in Figure 5 (right panel). The values of reduced χ^2 for these fits are 1.06, 1.13, 1.97, and 3.30.

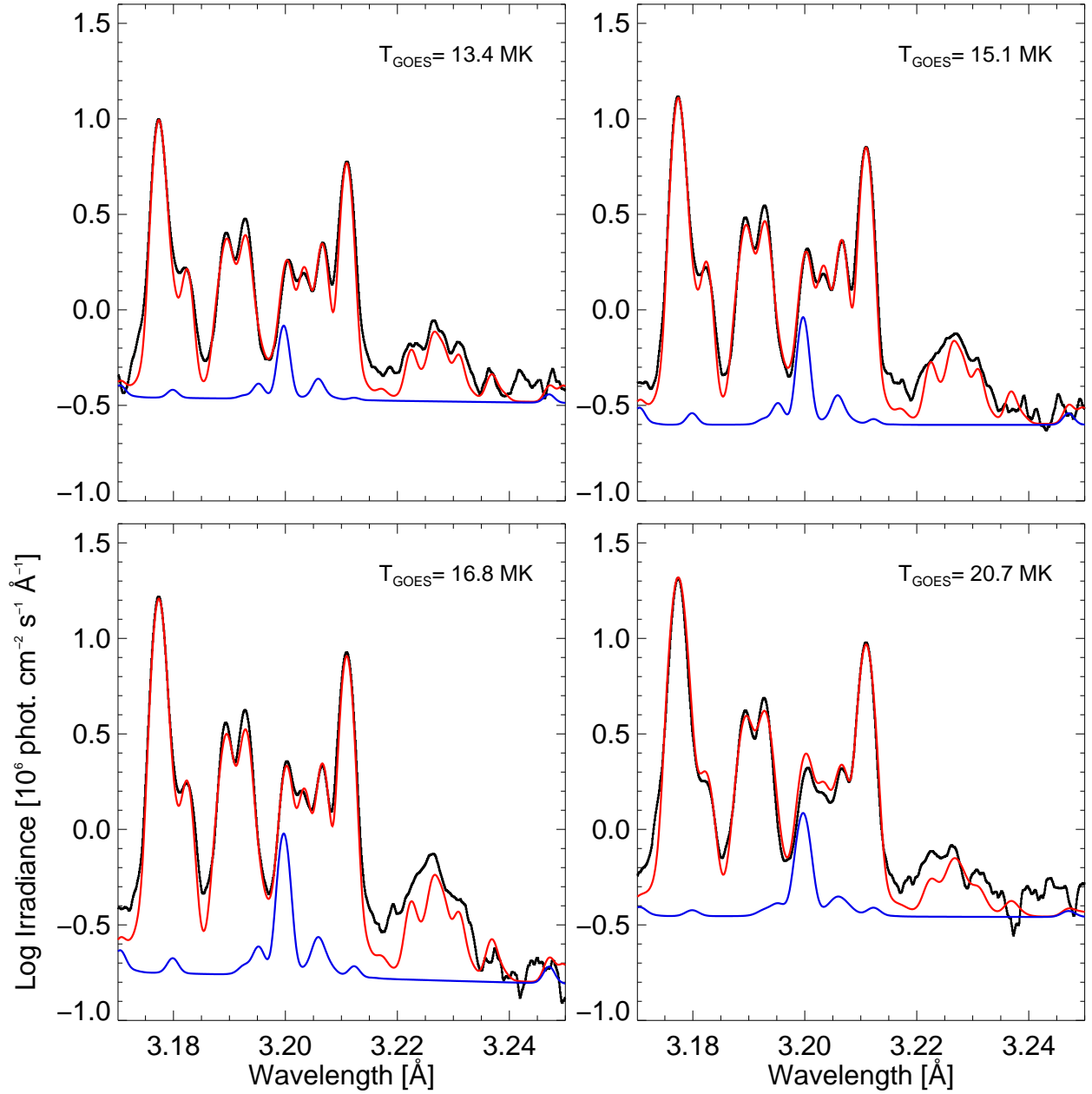


Fig. 7.— DIOGENESS spectra (3.17 – 3.25 \AA) for $T_{\text{GOES}} = 13.4$ MK, 14.8 MK, 16.8 MK, and 20.7 MK with best-fit theoretical spectra (red continuous line) with argon spectrum (blue line) for a wavelength range that includes only the region around the Ca XIX lines and Ca XVIII and Ca XVII satellites. The Ca^{+16} and Ca^{+17} ion fractions were multiplied by 1.3 and 2.0 respectively as in Figure 5. The values of reduced χ^2 for these fits are 2.41, 3.23, 5.84, and 9.86.

enhanced fluorescence. At the higher temperatures, the argon lines are more prominent, particularly the Ar XVIII Ly- β line at 3.151 Å, which are well fitted so verifying the CHIANTI atomic data on which the line intensities are based. The measured wavelengths of Rice et al. (2014) agree with the DIOGENESS wavelengths, which therefore validates the DIOGENESS wavelength scale.

When narrower (3.17 – 3.25 Å) wavelength ranges are chosen, the slightly discrepant intensities of the Ca XIX line y and to a smaller extent line x , in which the observed intensities are greater than the theoretical, are more apparent (Figure 7). This has been recognized in the past (e.g. Figure 5 of Bely-Dubau et al. (1982)) and also in fits to the equivalent Fe XXV lines (Lemen et al. 1984). High- n Ca XVIII satellites which converge on to these lines could possibly account for this, but in the synthetic spectral program this has been taken account of using the procedure of Bely-Dubau et al. (1979) in which the total intensity of each satellite group is proportional to n^{-3} and the peak wavelength is displaced from either x or y by an amount $\Delta\lambda$ which is proportional to n^{-3} . We used the Cowan calculations for the $n = 6$ satellites, calculated specifically, for the intensity and $\Delta\lambda$ for satellites with $n = 7$ to $n = 16$, as in Bely-Dubau et al. (1979). However, the amount of emission added was extremely small and did not account for the observed discrepancy. Unless it can be attributed to the Bely-Dubau et al. (1982) calculated collision strengths rather than more accurate close coupling data (see Section 3.2), the reason for the discrepancy remains unknown. In Figure 7, the Ca XVII line group is displayed to better advantage. Most of the satellite structure is accounted for by the present calculations, which give similar results to those of Seely & Doschek (1989). At higher temperatures, Ca XVIII satellite u becomes more prominent relative to the Ca XVII satellites, as is indicated in the DIOGENESS spectrum for 20.7 MK.

4.2. Solar Flare Spectra from P78-1 SOLFLEX

The computer program generating synthetic spectra in the region of the Ca XIX X-ray lines was written primarily to match the DIOGENESS spectra obtained in the large flare of 2001 August 25, but other spectra in which the Ca XIX lines and lower-ionization satellites are visible can be examined with the same program. These include high-resolution SOLFLEX spectra of the calcium lines from the *P78-1* spacecraft discussed by Doschek et al. (1979) and Seely & Doschek (1989). Four of these spectra were digitised and analyzed with the synthetic spectrum program including the same adjustments to the Ca^{+16} and Ca^{+17} ion fractions as discussed in Section 4.1. Figure 8 shows examples of four spectra from three large flares, with temperatures estimated from the intensity ratio of Ca XVIII satellite k to Ca XIX w . The line widths were broadened by a turbulent velocity of 60 km s^{-1} in all cases. With these isothermal fits, almost all the principal line features are reproduced in the synthetic spectra, including the main lines within the Ca XVII line group at $3.21 - 3.24 \text{ \AA}$, given in Table 1. Argon lines are apparent, particularly the Ar XVIII Ly- β line at 3.151 \AA and the weak Ar XVI A6 satellite feature (3.170 \AA) on the short-wavelength side of Ca XIX line w . The intensities of these lines in the theoretical spectra are very similar to the observed, so the Ar/Ca abundance ratio of 0.33 appears to apply to these spectra also. However, the mismatch of the Ca XIX lines x and y , as in the DIOGENESS spectra, occurs here, so indicating a problem in the calculation of the excitation of these lines and *not* the observations.

4.3. Alcator C-Mod Tokamak Spectra

High-resolution spectra of the calcium lines discussed here were obtained from an X-ray spectrometer viewing plasma produced in the Alcator C-Mod tokamak. They have been analyzed by Rice et al. (2014) and Rice et al. (2017). The measured electron density,

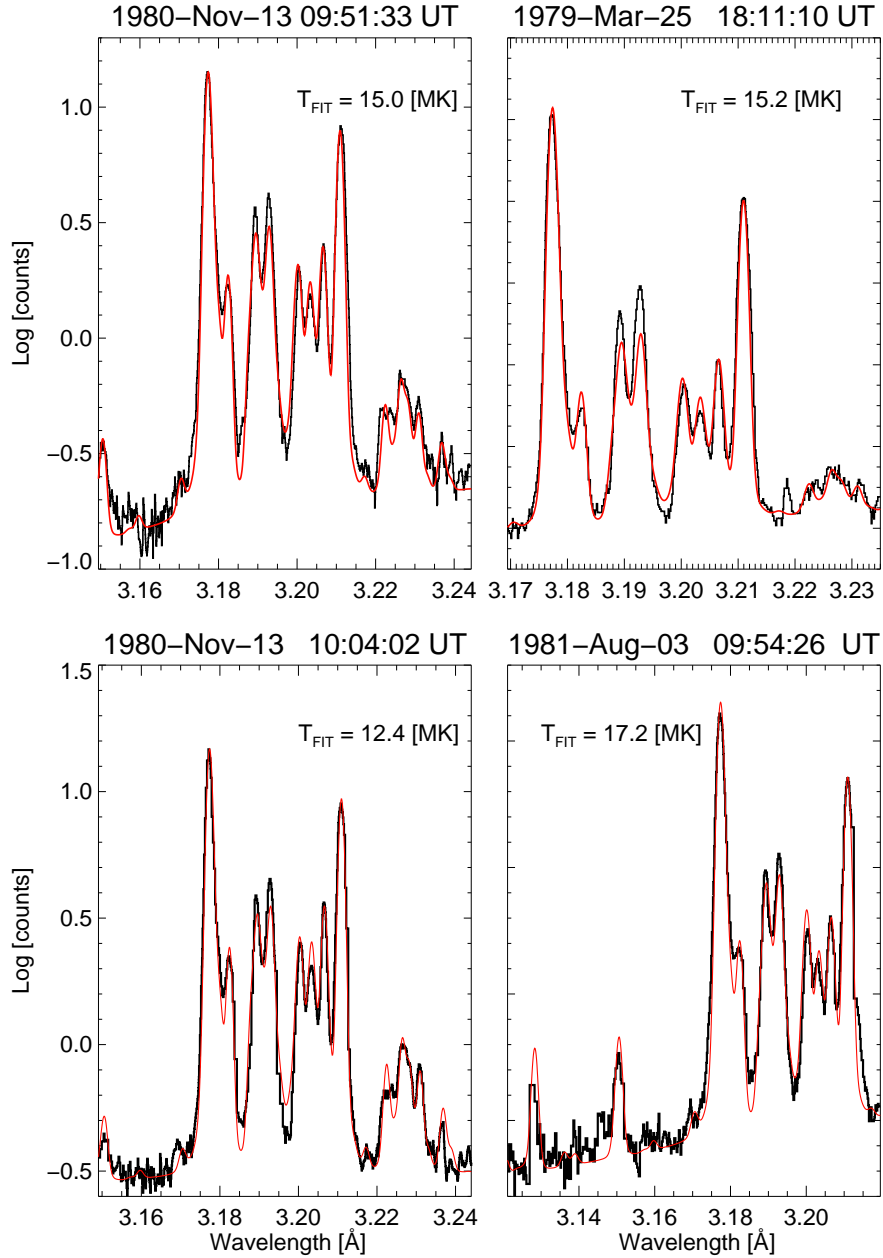


Fig. 8.— Four spectra from the *P78-1* SOLFLEX instrument during the flares of 1979 March 25, 1980 August 3 and 1981 November 13 (black lines) with spectral fits (red), with temperatures (indicated) from the Ca XVIII *k* line to Ca XIX *w* line ratio. The spectra were digitized from figures in Doschek et al. (1979) and Seely & Doschek (1989). The theoretical spectra (in red) are based on the *k/w* temperature and Ar/Ca abundance ratio of 0.33, with adjustments to the Ca^{+17} and Ca^{+16} ion fractions as discussed in the text.

$\sim 10^{14} \text{ cm}^{-3}$, at the center of the plasma is about a factor of 100 higher than those commonly measured in solar flare plasmas but the ionization and excitation conditions are similar. Two spectra shown in figures by Rice et al. (2014) were digitized and compared with synthetic spectra using only the calcium line spectra without the argon lines; they are shown in Figure 9. The top panel shows the spectrum viewed by the spectrometer through a central chord; the central temperature of the plasma was measured to be 3.5 keV (41 MK), much higher than any of the DIOGENESS or *P78-1* SOLFLEX solar flare spectra, though the presence of Ca XVIII satellites *q*, *r/a*, and *k* and even Ca XVII lines at wavelengths 3.22 – 3.23 Å suggests that lower-temperature plasma is present also, presumably along the line of sight of the spectrometer, either side of the plasma center. The observed line widths appear to be smaller than the thermal Doppler broadened values, which may indicate that the ion temperature is smaller than the electron temperature. A synthetic spectrum with a temperature of 25 MK approximately matches the observed, but Ca XVII satellite *q* is observed to be more intense than calculated, as are the Ca XVII satellites; this may be due to the assumption of a single temperature whereas lower-temperature plasma is also being viewed. In Figure 9 (lower panel), the spectrum was obtained by viewing the plasma at a distance of 0.5 times the distance from the plasma center to its edge and therefore shows a much lower temperature. We found an approximate fit with the synthetic spectrum having a temperature of 10.7 MK. The mismatches (e.g. in the Ca XVIII satellite *q* which is largely formed by inner-shell excitation rather than dielectronic recombination) may arise from lower-temperature plasma in the line of sight as in the higher-temperature spectrum.

5. RELATION OF Ca XIX AND *GOES* TEMPERATURES

We have assumed in the above analysis that an isothermal plasma with temperature T_{GOES} can describe DIOGENESS spectra adequately. Our experience with RESIK

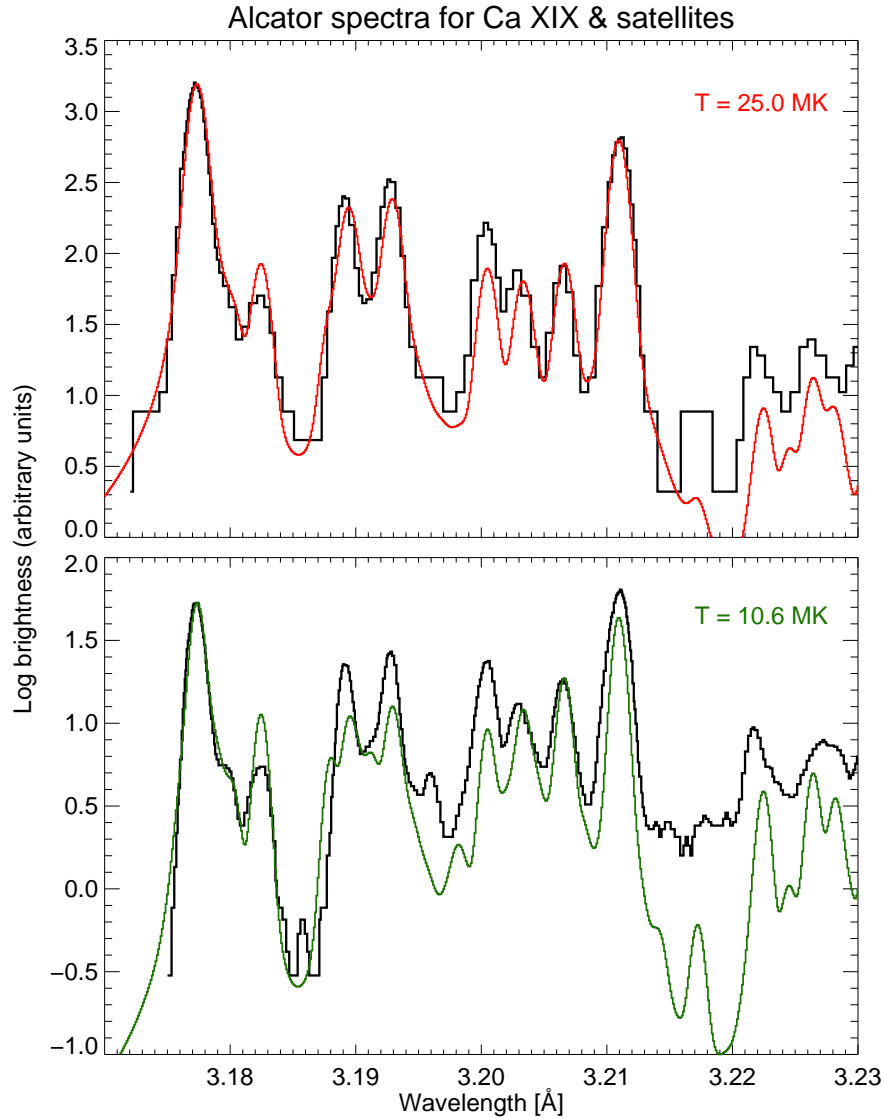


Fig. 9.— Two spectra in the neighborhood of the Ca XIX lines taken from the Alcator C-Mod tokamak, shown by Rice et al. (2014) and digitized here; the top panel is for the spectrometer viewing the plasma center, the lower panel at a distance half-way between the plasma center and its edge. The fitted synthetic spectra (red curves) have temperatures (in the figure legend) estimated from fitting the k/w line ratios as in Figure 8.

spectra has shown that this is a good approximation for describing K XIX and Ar XVII line emission including satellites (seen in RESIK channels 1 and 2) during flare decays (Sylwester et al. 2010b,a). An isothermal assumption was found to be less satisfactory during rapidly rising phases of flares. This agrees with an analysis of the late, nearly isothermal, stages of long-duration flares seen with the *Yohkoh* Bragg Crystal Spectrometer (Phillips et al. 2005). However, RESIK flare observations of the lower-temperature S XV, S XVI, and Si XIV line emission indicated a less satisfactory fit on an isothermal assumption (Sylwester et al. 2013), and instead a differential emission measure procedure was used to derive S and Si abundances (Sylwester et al. 2015a); T_{GOES} was found to be near the higher temperature range of the differential emission measure. A dependence on atomic number is thus suggested, an isothermal assumption with temperature equal to T_{GOES} adequately describing helium-like Ar ($Z = 18$) and K ($Z = 19$) line spectra during flare decays but not spectra from helium-like Si ($Z = 14$), S ($Z = 16$), and lower- Z elements for which lower-temperature plasma contributes to the line emission.

Here we examine the validity of an isothermal assumption for DIOGENESS Ca XIX spectra during the 2001 August 25 flare. We derived T_e from the temperature of the best fit (T_{FIT}) synthetic spectrum to each of sixty DIOGENESS spectra starting from scan 5 (see Figure 1, near the flare maximum and the maximum of the *Yohkoh* HXT signal). The values of T_{FIT} are plotted (black points) in Figure 10 (left panel) against time (UT), with corresponding values of T_{GOES} (red line). The precision of the later values of T_{FIT} is reduced as the flare spectra become less intense. A near-exact equality of the two temperatures is observed (Figure 10, right panel), the color code indicating temperature as well as time, with the higher temperatures measured at the earlier times. This is despite the fact that the earliest times include some non-thermal emission, as shown by HXT, which does not appear to affect the emission in either of the *GOES* channels. The use of T_{GOES} therefore appears to be justified by this analysis, which is consistent with our earlier work on K XIX

and Ar XVII line emission observed by RESIK.

6. SUMMARY AND CONCLUSIONS

We have here described X-ray spectra in the range of channels 1 and 4 of the DIOGENESS spectrometer on *CORONAS-F* during a powerful (X5) flare on 2001 August 25. The wavelength range, approximately $3.05 - 3.35 \text{ \AA}$, includes prominent lines of Ca XIX and associated dielectronic satellites and ionized argon (Ar XVII, Ar XVIII) lines including Ar XVI dielectronic satellites. The spectra were divided into five groups according to the value of T_{GOES} , the temperature obtained from the emission ratio of the two channels of *GOES*, which ranged from 12.8 MK to 20.7 MK. A computer program was used to synthesize the line spectrum based on atomic data of Bely-Dubau et al. (1982) for the Ca XIX lines, the Cowan Hartree–Fock code for the wavelengths and intensity factors for dielectronic satellites of Ca XVIII, Ca XVII, and Ca XVI, atomic data for the Ar XVII and Ar XVIII lines from CHIANTI, and the Cowan code for associated dielectronic satellites. Table 1 lists the more intense lines included in the synthetic spectral calculation which included over 2000 lines. Comparison with the DIOGENESS spectra averaged over the five temperature intervals shows good agreement for the Ca XIX and Ca XVIII satellites, but the Ca XVII and weaker Ca XVI satellites were found to be more intense in the DIOGENESS spectra. The argon lines were generally well fitted by the synthetic spectra. By increasing the Ca^{+17} and Ca^{+16} ion fractions by factors of 1.3 and 2.0 respectively, much improved agreement was achieved. This adjustment of the ion fractions is justified by the fact that the Ca^{+17} and Ca^{+16} ion fractions are small at all relevant temperatures, and a roughly 10% uncertainty in ionization and recombination rates would easily explain such increases. Comparison of synthetic spectra with those from the *P78-1* SOLFLEX instrument (Figure 8) shows good agreement, although comparison with the calcium spectra

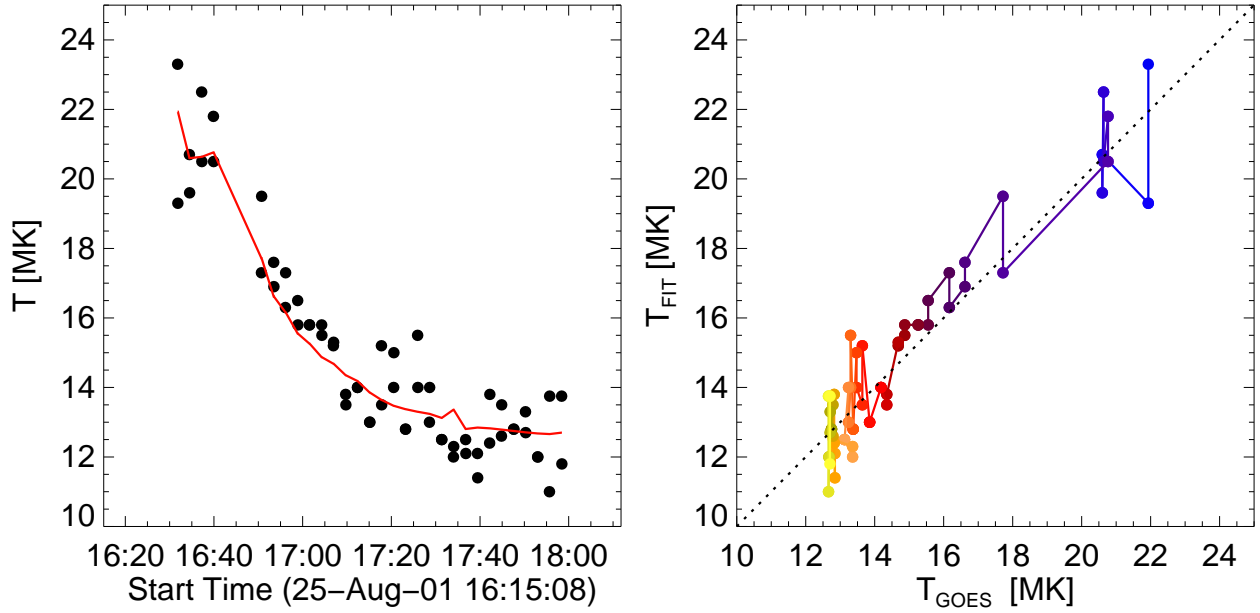


Fig. 10.— Left: Temperature (T_{FIT}) (black dots) estimated from the fit to each DIOGENESS spectrum for spectra starting at scan 5 during the 2001 August 25 flare and T_{GOES} plotted against time. Right: T_{FIT} plotted against T_{GOES} (colored dots) for the same time period, blue dots indicating higher temperatures (earlier times), lighter colors lower temperatures (later times). The dashed line indicates equal temperatures.

produced in the Alcator C-Mod tokamak are slightly less satisfactory, the explanation probably being the multi-thermal and non-equilibrium or non-stationary nature of the plasma.

From the synthetic spectra, we find that the overlap of ionized calcium and argon lines in the spectral range of interest is important in at least one case, the blend of the Ca XVIII satellite q (3.2005 Å), commonly used to diagnose the non-equilibrium state of flare plasmas (Bely-Dubau et al. 1982), with the Ar XVII $w4$ line (3.1997 Å), as was pointed out by Doschek & Feldman (1981). With an assumed Ar/Ca ratio of 0.33 (based on measurements by Sylwester et al. (1998) and Sylwester et al. (2010a)), the contribution made by the Ar XVII line is comparable to the q line. As pointed out by Sylwester et al. (1998), the calcium abundance varies from flare to flare, so the blend may be more or less serious according as the calcium abundance is less or more; an extreme case has been pointed out by Doschek & Warren (2016) who find from ultraviolet line emission near a sunspot that the Ar/Ca abundance ratio may be more than photospheric, equal to around 1.4. On the other hand, a large enhancement of the calcium abundance might occur in flares on active dwarf M stars, if the FIP effect is larger than that apparently operating in the solar atmosphere; thus, the Ar/Ca abundance ratio may be less than our assumed value, reducing the effect of argon line blends. It should be noted also that line blends occur in other X-ray spectral regions, e.g. with the S XV $w6$ line (3.998 Å) very near the Ar XVII lines at 3.969 – 3.994 Å. These may be relevant to observations of stellar coronae taken with the *Chandra* High Energy Transmission Grating Spectrometer.

Weaker Ar XVI satellites in DIOGENESS spectra make small contributions, e.g. the A5 feature (3.2058 Å) makes a few percent contribution to Ca XVIII line k (3.2066 Å), and the A6 feature (3.1704 Å) may appear on the short-wavelength side of the Ca XIX line w (3.1774 Å). With the very high sensitivity and spectral resolution of DIOGENESS, the

weak Ar XVI satellite features A6 and A4 (3.273 Å) and the Ca XVIII *p* and *o* satellites (3.2636 Å, 3.2688 Å) are evident, particularly in the spectrum with $T_{\text{GOES}} = 16.8$ MK. These lines have not been recorded in solar flare spectra before.

We have also examined the assumption of isothermal plasma to describe the DIOGENESS spectra, plotting the temperature (T_{FIT}) of the best-fit synthetic spectrum to each DIOGENESS spectrum from scan 5 to the end of the observations against T_{GOES} , finding an almost exact equality. An isothermal description of Ca XIX emission is therefore valid, with the temperature given by T_{GOES} .

Although solar flare X-ray spectra in the region of the Ca XIX lines have not recently been observed, analysis of the extensive archive of *SMM* BCS spectra is now possible with application of the synthetic spectral code described here. In particular, it will be possible to re-analyze spectra used to derive the flare calcium abundance and deduce more exactly the relation of the variability of this abundance with flare type; this analysis is now proceeding. Future spacecraft instrumentation – the ChemiX spectrometer, due for launch on *Interhelioprobe* in 2025 or 2026 – will benefit from the synthetic spectral procedure described here.

We acknowledge financial support from the Polish National Science Centre grant numbers UMO-2013-11/B/ST9/00234 and UMO-2017/25/B/ST9/01821. We acknowledge the help of Jarek Bakała in digitizing the *P78-1* and Alcator spectra, Żaneta Szaforz for calculating the total quartz crystal reflectivities using the XOP package, and Marek Śteślicki for reformatting the DIOGENESS telemetry. The CHIANTI atomic database and code is a collaborative project involving George Mason University, University of Michigan (USA), and University of Cambridge (UK).

Facilities: GOES, CORONAS/DIOGENESS, CORONAS/RESIK, Yohkoh/HXT,

Yohkoh/SXT

REFERENCES

- Aggarwal, K. M., & Keenan, F. P. 2012, *Phys. Scr*, 85, 025306
- Asplund, M., Grevesse, N., Sauval, A. J., & Scott, P. 2009, *Ann. Rev. Astr. Astroph.*, 47, 481
- Bely-Dubau, F., Faucher, P., Steenman-Clark, L., Dubau, J., Loulergue, M., Gabriel, A. H., Antonucci, E., Volonte, S., & Rapley, C. G. 1982, *MNRAS*, 201, 1155
- Bely-Dubau, F., Gabriel, A. H., & Volonte, S. 1979, *MNRAS*, 189, 801
- Bryans, P., Badnell, N. R., Gorczyca, T. W., Laming, J. M., Mitthumsiri, W., & Savin, D. W. 2006, *ApJS*, 167, 343
- Bryans, P., Landi, E., & Savin, D. W. 2009, *ApJ*, 691, 1540
- Burgess, A., & Tully, J. A. 1992, *A&A*, 254, 436
- Cowan, R. D. 1981, *The theory of atomic structure and spectra* (Berkeley: University of California Press, 1981)
- Del Zanna, G., Dere, K. P., Young, P. R., Landi, E., & Mason, H. E. 2015, *A&A*, 582, A56
- Dere, K. P., Landi, E., Mason, H. E., Monsignori Fossi, B. C., & Young, P. R. 1997, *A&AS*, 125, 149
- Doschek, G. A., & Feldman, U. 1981, *ApJ*, 251, 792
- Doschek, G. A., Kreplin, R. W., & Feldman, U. 1979, *ApJ*, 233, L157
- Doschek, G. A., & Warren, H. P. 2016, *ApJ*, 825, 36
- Erickson, G. W. 1977, *Journal of Physical and Chemical Reference Data*, 6, 831

- Feldman, U. 1992, *Phys. Scr.*, 46, 202
- Feldman, U., Doschek, G. A., Nagel, D. J., Cowan, R. D., & Whitlock, R. R. 1974, *ApJ*, 192, 213
- Gabriel, A. H. 1972, *MNRAS*, 160, 99
- Landi, E., Del Zanna, G., Young, P. R., Dere, K. P., Mason, H. E., & Landini, M. 2006, *ApJS*, 162, 261
- Lemen, J. R., Phillips, K. J. H., Cowan, R. D., Hata, J., & Grant, I. P. 1984, *A&A*, 135, 313
- Mann, J. B. 1983, *Atomic Data and Nuclear Data Tables*, 29, 407
- Merts, A. L., Cowan, R. D., & Magee, Jr., N. H. 1976, Los Alamos Report UC-20 (LA-6220-MS), Tech. rep., Los Alamos Scientific Laboratory, N.M.
- Phillips, K. J. H., Feldman, U., & Harra, L. K. 2005, *ApJ*, 634, 641
- Phillips, K. J. H., Feldman, U., & Landi, E. 2008, *Ultraviolet and X-ray Spectroscopy of the Solar Atmosphere* (Cambridge University Press)
- Rice, J. E., Fournier, K. B., Safronova, U. I., Goetz, J. A., Gutmann, S., Hubbard, A. E., Irby, J., LaBombard, B., Marmar, E. S., & Terry, J. L. 2017, Unpublished preprint
- Rice, J. E., Reinke, M. L., Ashbourn, J. M. A., Gao, C., Bitter, M., Delgado-Aparicio, L., Hill, K., Howard, N. T., Hughes, J. W., & Safronova, U. I. 2015, *Journal of Physics B Atomic Molecular Physics*, 48, 144013
- Rice, J. E., Reinke, M. L., Ashbourn, J. M. A., Gao, C., Victora, M. M., Chilenski, M. A., Delgado-Aparicio, L., Howard, N. T., Hubbard, A. E., Hughes, J. W., & Irby, J. H. 2014, *J. Phys. B Atom. Mol. Phys.*, 47, 075701

- Safronova, U. I., & Lisina, T. G. 1979, *Atomic Data and Nuclear Data Tables*, 24, 49
- Sanchez del Rio, M., & Dejus, R. J. 2004, in *Proc. SPIE*, Vol. 5536, *Advances in Computational Methods for X-Ray and Neutron Optics*, ed. M. Sanchez del Rio, 171–174
- Seely, J. F., & Doschek, G. A. 1989, *ApJ*, 338, 567
- Siarkowski, M., & Falewicz, R. 2004, *A&A*, 428, 219
- Siarkowski, M., Sylwester, J., Bakała, J., Szaforz, Ż., Kowaliński, M., Kordylewski, Z., Płoceniak, S., Podgórski, P., Sylwester, B., Trzebiński, W., Stęślicki, M., Phillips, K. J. H., Dudnik, O. V., Kurbatov, E., Kuznetsov, V. D., Kuzin, S., & Zimovets, I. V. 2016, *Experimental Astronomy*, 41, 327
- Sylwester, B., Phillips, K. J. H., Sylwester, J., & Kępa, A. 2013, *Sol. Phys.*, 283, 453
- . 2015a, *ApJ*, 805, 49
- Sylwester, B., Phillips, K. J. H., Sylwester, J., & Kuznetsov, V. D. 2011, *ApJ*, 738, 49
- Sylwester, J., Gaicki, I., Kordylewski, Z., Kowaliński, M., Nowak, S., Płoceniak, S., Siarkowski, M., Sylwester, B., Trzebiński, W., Bakała, J., Culhane, J. L., Whyndham, M., Bentley, R. D., Guttridge, P. R., Phillips, K. J. H., Lang, J., Brown, C. M., Doschek, G. A., Kuznetsov, V. D., Oraevsky, V. N., Stepanov, A. I., & Lisin, D. V. 2005, *Sol. Phys.*, 226, 45
- Sylwester, J., Kordylewski, Z., Płoceniak, S., Siarkowski, M., Kowaliński, M., Nowak, S., Trzebiński, W., Stęślicki, M., Sylwester, B., Stańczyk, E., Zawerbny, R., Szaforz, Ż., Phillips, K. J. H., Fárník, F., & Stepanov, A. 2015b, *Sol. Phys.*, 290, 3683
- Sylwester, J., Lemen, J. R., Bentley, R. D., Fludra, A., & Zolcinski, M.-C. 1998, *ApJ*, 501, 397

Sylwester, J., Sylwester, B., Phillips, K. J. H., & Kuznetsov, V. D. 2010a, *ApJ*, 720, 1721

—. 2010b, *ApJ*, 710, 804

—. 2012, *ApJ*, 751, 103

Vainshtein, L. A., & Safronova, U. I. 1978, *Atomic Data and Nuclear Data Tables*, 21, 49

Whiteford, A. D., Badnell, N. R., Ballance, C. P., O’Mullane, M. G., Summers, H. P., & Thomas, A. L. 2001, *Journal of Physics B Atomic Molecular Physics*, 34, 3179